Sana Toumi[1,2], Elhoussin Elbouchikhi[3], Mohamed Benbouzid[2,4] Yassine Amirat[3]

J. Electrical Systems 16-4 (2020): 429-447

Regular paper

Grid Fault-Resilient Control of a PMSG-based Tidal Stream Turbine

Journal of Electrical Systems

This paper describes a grid fault-resilient control approach for a grid-connected tidal stream turbine (TST) driven by a permanent magnet synchronous generator (PMSG). TSTs mainly use conventional PI controllers while they are very sensitive to grid faulty conditions. In this faulty context, the TST will experience power generation decrease and dynamic performance degradations. Indeed, the grid-side converter can be deactivated and the generator may be disconnected from the grid. Also, grid faults can make the system instable during and after faults occurrence, which can deteriorate the quality of the power injected into the grid from the TST generation system. In this paper, a resilient controller is therefore derived to enhance the PMSG-based TST performance during grid fault. In fact, high-order sliding modes have been adopted to sustain a minimum level of optimal performance and achieve a smoother grid-injected power in case of a grid fault. Simulations carried out on real tidal speed data measured at the Raz de Sein site in Bretagne in France clearly highlights proves the effectiveness of the proposed grid fault-resilient approach.

Keywords: Tidal stream turbine; permanent magnet synchronous generator, generator-side converter; grid-side converter; LVRT; fault-resilient control; PI control; second-order sliding mode control.

Article history: Received 20 April 2020, Accepted 15 July 2020

1. Introduction

In recent years, the use of renewable energy sources such as thermal energy, wave energy and marine tidal energy offers the advantage of sustainability in all aspects of the energy sector development. In fact, marine tidal energy pioneer projects have experienced a fast development. These projects are mainly due to huge tidal energy potential in Europe. In fact, there is 42% of the European tidal energy in France, 48% in the UK, and 8% in Ireland [1-2].

Unfortunately, tidal turbines are underwater systems and are, therefore, affected by several failures due to the marine harsh environment and the weather conditions such as grid faults. Indeed, grid faults are mainly due to weather conditions (37% of grid faults causes are related to weather conditions in Iceland, 23% in Denmark and 21% in Norway) [3]. Figure 1 represents different types of grid faults such as single line-to-ground short-circuit fault (Fig. 1.a), line-to-line short-circuit fault (Fig. 1.b), line-to-line-to-ground short-circuit fault (Fig. 1.c), and three phases short-circuit fault (Fig. 1.d). Short-circuit fault can defined by its duration and its amplitude. In fact, fault duration depends on the time taken by the protection systems to detect and isolate the fault. In general, a fault takes a few hundreds of milliseconds [4]. Short-circuit fault present a grid voltage variation (voltage drops or overvoltage). Under normal conditions, grid voltage fluctuates around its nominal value with a variation of ±10% of this value. So, grid fault voltage variation amplitude is between 10% and 90% of nominal grid voltage [5].

Short-circuit faults in the power grid have disturbing effects on optimal operation of grid-connected marine turbine systems. The impact of grid faults on TSTs performance

* Corresponding author: Mohamed Benbouzid, E-mail: Mohamed.Benbouzid@univ-brest.fr
[1]University of Sousse, ENISO, LASEE, 4023, Sousse, Tunisia (e-mail: sanaatoumii@gmail.com)
[2]University of Brest, UMR CNRS 6027 IRDL, 29238, Brest, France (e-mail: Mohamed.Benbouzid@univ-brest.fr)
[3]ISEN Yncréa Ouest, UMR CNRS 29200, Brest, France (e-mails: elhoussin.elbouchikhi@isen-ouest.yncrea.fr; yassine.amirat@isen-ouest.yncrea.fr)
[4]Shanghai Maritime University, 201306 Shanghai, China

depends on the grid fault severity. Indeed, grid faults can cause a high stator currents, which, can damage the generator windings insulation and can be harmful for grid-side converter switching and greatly increase the DC-link voltage, which may lead to DC bus break down. In these conditions, the grid-side converter can be deactivated and the generator may be disconnected from the grid for a safe shutdown of the whole system. Before emergency breakage activated, this kind of grid faults can make the system instable during and after faults occurrence, which can lead to catastrophic failure and irreversible damage to the TST subsystems [6].

Also, short-circuit grids faults could cause frequency and voltage control issues in the system, hence providing large power grid ripple and increasing current harmonics distortion [7]. Consequently, it results in deteriorating the quality of the power injected to the grid from the TST generation system.

In order to ensure the continuous operation of the TSTs after a fault occurrence, low voltage ride-through (LVRT) methods are widely discussed in the literature [8-9]. Indeed, LVRT methods are generally divided into two categories: the first one is based on the use of auxiliary elements such as energy storage system, crowbar protection system, flexible alternating current transmission system (FACTS devices) [10-11]. The second category is based on using fault-resilient control approaches as discussed in [12-13].

Regarding the first category, a supercapacitor is used as an energy storage system device in order to smooth power fluctuations and improve the LVRT capability of the energy conversion system in [14]. Indeed, the difference between the produced power and the injected power to the grid is stored in the supercapacitor for power smoothing [15]. In [16], the supercapacitor is used as an energy storage system combined with an innovative control approach based on a model predictive control technique for output power smoothing. In [17-18], the crowbar protection system has been used to limit the rotor short-circuit current and make the rotor-side converter deactivated during the fault and keeps it off until the stator voltage is recovered. In [19-20], the crowbar system is composed by a high power resistor in series with switches for safe shutdown of the overall system. It is used to dissipate the active power during faulty conditions. This system is known with its advantages as simple circuit topology and low cost. However, it can not improve the injection of the reactive power to the grid unless it is combined with other methods [21-22].

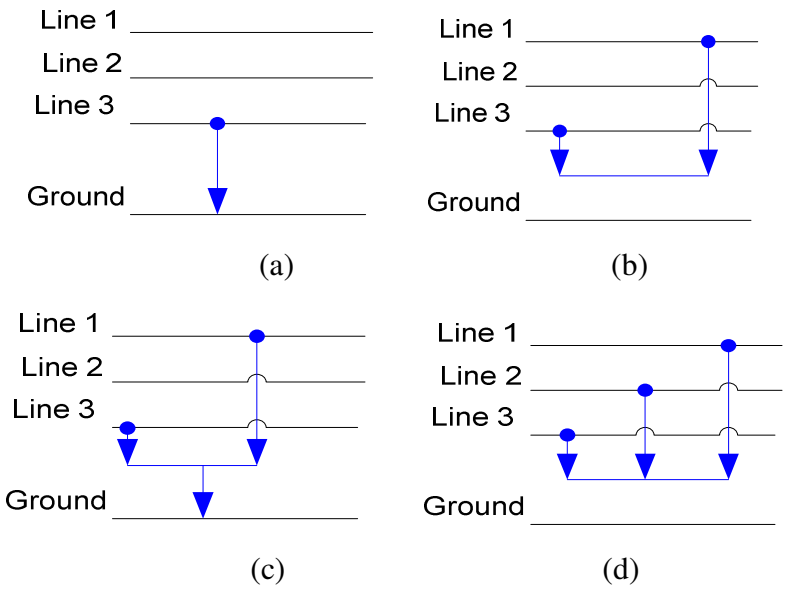

Fig. 1.(a) Single line-to-ground short-circuit fault, (b) Line-to-line short-circuit fault, (c) Line-to-line-to-ground short-circuit fault, (d) Three phases short-circuit fault.

Moreover, FACTS devices keep systems connected to the grid even at faulty conditions [23-24]. Indeed, in [25], an additional series-connected voltage source converter (VSC) at the generator terminal has been inserted. These systems present a large number of switches, which makes it expensive.

In the case of grid faults, conventional control techniques such as PI controllers are very sensitive to faulty conditions and their consequences. Therefore, the second category of LVRT based on robust fault-resilient control techniques is required. In the literature, many fault-resilient control strategies have been proposed. These strategies are applied to the generator-side converter [26] but also to the grid-side converter [27] to avoid disconnection of the marine current turbine during grid faults conditions. In [28], authors proposed a new control strategy to improve the fault-ride through (FRT) capacity of generator during symmetric and asymmetric grid disturbances. This strategy is based on active and passive LVRT compensators. The active compensator is used to determinate the appropriate references currents at fault occurrence in order to reduce overvoltage. The passive compensator is based on a rotor current limiter to reduce transient currents. By applying this strategy, electromagnetic torque oscillations and overvoltage in the DC link are reduced. In [29], the proposed control strategy is based on the addition of a hysteresis current regulator to protect the machine against severe voltage drop.

To guarantee system stability, in the case of grid faults, the authors proposed in [30] a control strategy based on the combination of the stator flux and the rotor flux. In [31], the proposed strategy is based on the damping of virtual flux in order to eliminate system disturbances. In [32], the authors proposed a new control strategy using genetic algorithms.

In this context, the main objective of this paper is to prove the limitations of the conventional PI controllers technique for the tidal turbine resilience under grid faulty conditions. Then, a second-order sliding mode control strategy is proposed and demonstrated to be robust and efficient for the tidal turbine resilience under grid faulty conditions.

In this paper, a 1.5MW grid-connected PMSG-based TST is studied. The remaining parts of this paper are organized as follows: Section II describes the grid-connected tidal turbine system modeling including the resource, the turbine rotor, the PMSG, the two converters, and the grid. Section III, describes the grid-connected tidal turbine system control using PI controllers. Section IV presents the grid-connected tidal turbine system control using second-order sliding mode control. Section V illustrates some simulation results. Finally, section VI concludes this paper.

2. Grid-connected tidal turbine modeling

Figure 2 represents the basic structure of a tidal turbine connected to the grid. This structure is composed of a turbine rotor, a permanent magnet synchronous generator coupled to a DC-bus via a three-phase converter (rectifier). The connection to the grid is achieved based on a three-phase converter (inverter) and LC filter.

2.1. Resource modeling

Marine currents are created by the gravitational interaction of the moon, the sun and the earth [33], which causes seawater motion regularly each day with a period of approximately 12 h and 24 min (a semi diurnal tide), or with a period of about 24 h and 48 min (a diurnal tide). In France, tidal current data are given by the SHOM (French Navy Hydrographic and Oceanographic Service), and are available for different locations in chart form [34]. Therefore, knowing tide coefficient, it is easy to derive a simple and practical model for tidal current velocities v_t [35].

$$v_t = v_{nt} + \frac{(C-45)(v_{st}-v_{nt})}{95-45} \quad (1)$$

Where C corresponds to the tide coefficient, which characterize each tidal cycle, (95 and 45 are the spring and neap tide medium coefficients, respectively). v_{st} and v_{nt} are the spring and neap tide current velocities, respectively. The first-order model is used to calculate the tidal velocity for each second.

2.2. Tidal turbine model

The mechanical power for a tidal stream turbine is given by [36-37]

$$P_m = \frac{1}{2} C_p(\lambda, \beta) \rho \pi r^2 v_t^3 \quad (2)$$

where ρ is fluid density, r is the turbine radius, v_t is the tidal velocity, and $C_p(\lambda, \beta)$ is the power coefficient, which depends on the turbine blade structure and its hydrodynamics. For typical tidal turbines, the maximum value of C_p for normal operation is estimated to be in the range of 0.35-0.5 [38]. Indeed, based on experimental results and for a given turbine, the C_p can be approximated by an equation depending on the tip speed ratio λ and the blade pitch angle β [39-40]. In this paper, the TST is not pitched. In this context, the C_p is supposed to be only depending on λ. Figure 3 illustrates the C_p curve used for simulations. In order to extract the maximum of mechanical power from the fluid stream, the power coefficient must be at its maximum value C_{pmax}= 0.45, which corresponds to the optimal tip speed ratio λ = 6.3.

2.3. Permanent magnet synchronous generator modeling

In term of generator option, the PMSG is a promising solution for underwater applications [41]. In fact, it has many advantages such as compactness, higher efficiency, and the possibility to eliminate the gearbox, thus reducing maintenance costs [42].

The PMSG dynamic model, in the *d-q* frame, is given by [43]

$$\begin{cases} J_t \frac{d\Omega}{dt} = T_m - T_{em} - f\Omega \\ \frac{di_{sd}}{dt} = -\frac{R_s}{L_s} i_{sd} + p\Omega i_{sq} + \frac{v_{sd}}{L_s} \\ \frac{di_{sq}}{dt} = -\frac{R_s}{L_s} i_{sq} - p\Omega i_{sd} - p\frac{\Phi_a}{L_s} + \frac{v_{sq}}{L_s} \end{cases} \quad (3)$$

where v_{sd} and v_{sq} are the d-q components of the stator voltages respectively, i_{sd} and i_{sq} are the d-q components of the stator currents, respectively. R_s is the stator resistance, L_s is the stator inductance, Φ_a is the permanent magnet flux, p is the pole-pairs number, Ω is the turbine speed, T_{em} is the electromagnetic torque, T_m is the mechanical torque, J_t is the turbine and PMSG total inertia, and f is the viscosity coefficient.

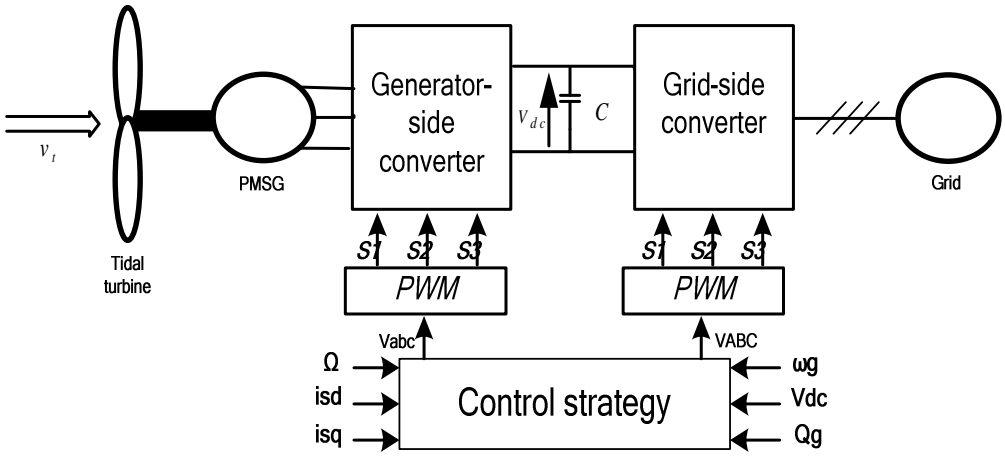

Fig. 2. Grid-connected PMSG-based tidal stream turbine system basic structure.

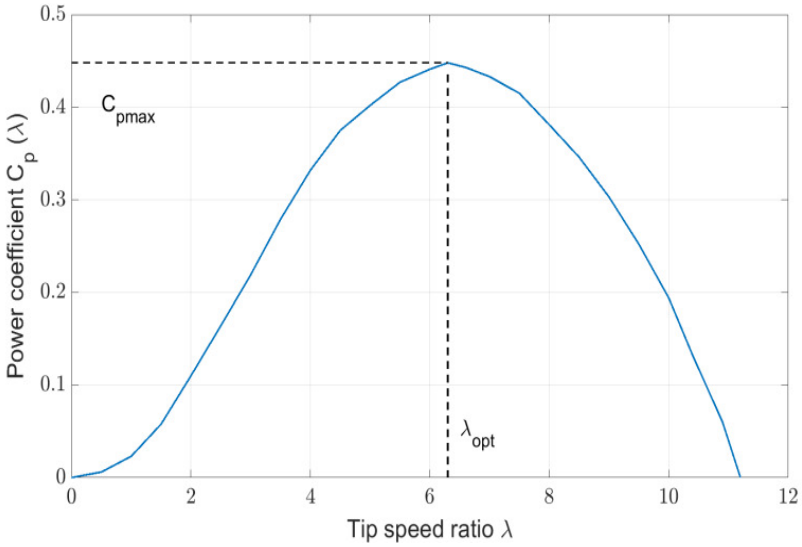

Fig. 3. Tidal stream turbine power coefficient curve.

2.4. Power converters modeling

The grid-connected tidal stream turbine uses two power converters; the first one is connected to the generator (rectifier), and the second is connected to the grid (inverter). The two power converters have the same structure as shown by Fig. 4, it is composed by three legs using two semiconductor switches (T_k, T_{k+3}, k=1, 2, 3) with anti-parallel connected freewheeling diodes (D_k, D_{k+3}). The switches of the same leg are controlled by a PWM using logic control signals S_k (k = 1, 2, 3) also known as gate signals [44]. The k^{th} gate signal denoted S_k switch is defined by

$$S_k = \begin{cases} 1 \text{ if } T_k \text{ on and } T_{k+3} \text{ off} \\ 0 \text{ if } T_{k+3} \text{ on and } T_k \text{ off} \end{cases} \quad (4)$$

2.5.DC-bus modeling

The DC-bus model is described as follows:

$$\frac{dV_{dc}}{dt} = \frac{1}{C}(i_1 - i_2) \tag{5}$$

where *C* is the capacitor.

2.6. Grid-side converter modeling

As shown by Fig.5, the grid is composed by a voltage V_g with a frequency f = 50Hz [45].The grid dynamic model, in the *abc* frame, is given as follows:

$$\begin{pmatrix} V_A \\ V_B \\ V_C \end{pmatrix} = \mathrm{R_g}\begin{pmatrix} I_{g1} \\ I_{g2} \\ I_{g3} \end{pmatrix} + \mathrm{L_g}\frac{\mathrm{d}}{\mathrm{dt}}\begin{pmatrix} I_{g1} \\ I_{g2} \\ I_{g3} \end{pmatrix} + \begin{pmatrix} V_{g1} \\ V_{g2} \\ V_{g3} \end{pmatrix} \tag{6}$$

where V_{g123} and I_{g123} are the grid line voltages and currents respectively, V_{ABC} are the converter voltages.

The grid dynamic model, in the *d-q* frame, is summarized by [46]

$$\begin{cases} V_{od} = R_g I_{gd} + L_g \frac{dI_{gd}}{dt} - L_g \omega_g I_{gq} + V_{gd} \\ V_{oq} = R_g I_{gq} + L_g \frac{dI_{gq}}{dt} + L_g \omega_g V_{gd} + V_{gq} \end{cases} \tag{7}$$

where v_{gd} and v_{gq} are the d-q components of the grid voltages, respectively. i_{gd} and i_{gq} are the *d-q* components of the grid currents, respectively. ω_g is the grid angular frequency.

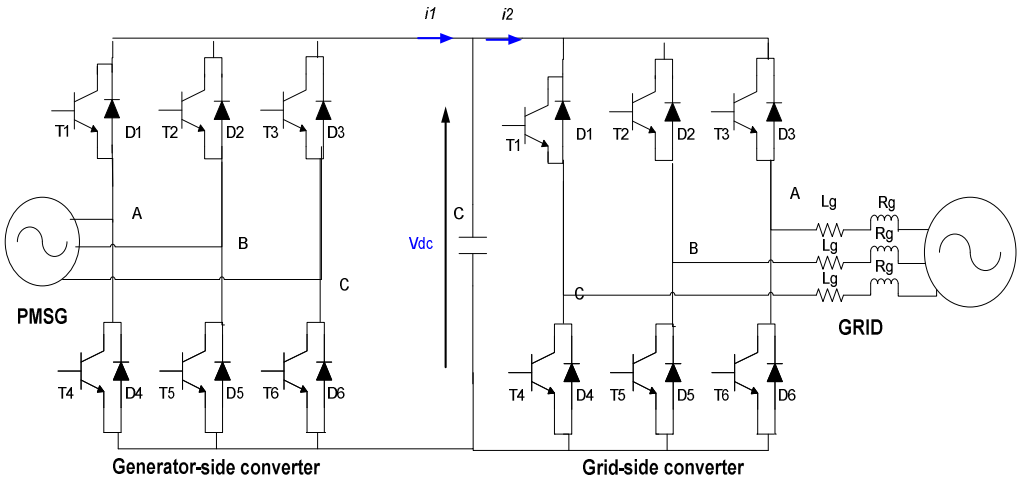

Fig. 4. Power converters topology.

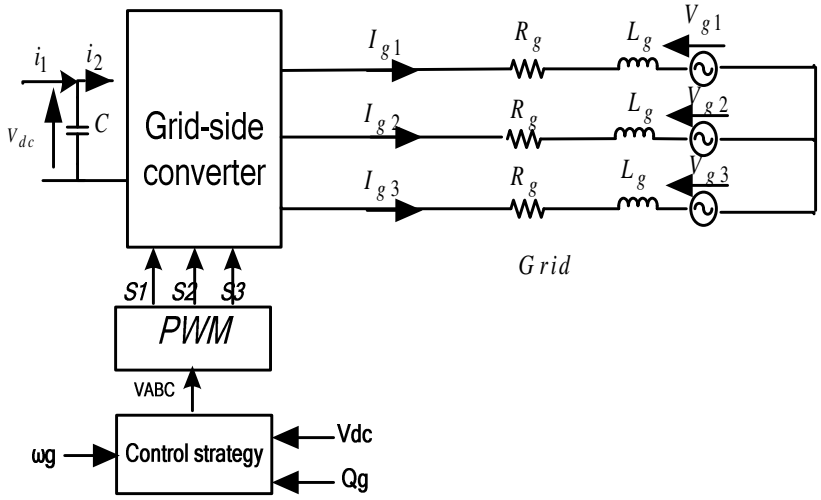

Fig. 5. Grid topology.

3. Grid-connected PMSG-based tidal stream turbine PI control

The grid-connected PMSG-based TST must have two controls: (1) The generator-side control: it maintains the conversion system at its maximum power point to extract the maximum energy from tidal currents; (2) The grid-side control: it aims to control active and reactive power injected to the grid and keep the DC-bus voltage constant.

3.1. Generator-side converter control

The generator-side control system is based on PI controllers. It is defined as follows:

$$\begin{cases} i_{sd} = \frac{1}{R_s + L_s s}(v_{sd} + \omega\psi_{sq}) \\ i_{sq} = \frac{1}{R_s + L_s s}(v_{sq} - \omega\psi_{sd}) \end{cases} \tag{8}$$

where ω is the electrical speed, ψ_{sq}, and ψ_{sq} are the d-q components of the PMSG flux, respectively and are given by

$$\begin{cases} \psi_{sd} = L_s i_{sd} + \Phi_a \\ \psi_{sq} = L_s i_{sq} \end{cases} \tag{9}$$

The electromagnetic torque is given by

$$T_{em} = \frac{3}{2} p \Phi_a i_{sq} \tag{10}$$

Figure 6 illustrates the generator side-control scheme. In fact, it mainly consists in a Maximum Power Point Tracking (MPPT) control, which is used to control the rotor speed and keep the turbine tip speed ratio λ at its optimal value in order to achieve a maximum value of the power coefficient C_p and to finally obtain the expected maximum power from

the TST. Indeed, the turbine speed reference calculated by MPPT technique is given by [39].

$$\Omega_{ref} = \frac{v_t \lambda_{opt}}{r} \tag{11}$$

Thus, the reference of the rotational speed control loop is adjusted so that the turbine will operate around the maximum power for the given tidal speed. In this paper, the turbine maximum speed to follow MPPT is 25 rpm for a tidal current of 2.3 m/s. If the tidal velocity exceeds 2.3m/sec, the extracted power will be limited to 1.5MW.

3.1.1. PI speed controller

The PI speed controller is given by

$$R(s) = b_1 + \frac{b_0}{s} \tag{12}$$

where b_0 and b_1 are the speed controller integral and proportional gains, respectively. Using Eq. (3), the turbine speed control structure is given by Fig. 7.

In closed-loop, the transfer function is given by

$$F_\Omega(s) = \frac{b_0 + b_1 s}{J_t s^2 + s(f + b_1) + b_0} \tag{13}$$

Compared to the canonical form expressed by

$$F(s) = \frac{k}{\frac{1}{\omega_0^2} s^2 + \frac{2\xi}{\omega_0} s + 1} \tag{14}$$

where ω_0 is the angular frequency and ξ is the damping factor.

By identification, the turbine speed corrector parameters are given as:

$$\frac{1}{b_0} = \frac{1}{\omega_0^2} \leftrightarrow b_0 = J_t \omega_0^2 \tag{15}$$

$$\frac{f + b_1}{b_0} = \frac{2\xi}{\omega_0} \leftrightarrow b_1 = \frac{2\xi b_0}{\omega_0} - f \tag{16}$$

3.1.2. PI currents controllers

The PI current controller is given by

$$R(s) = K_p \left(1 + \frac{1}{K_i s}\right) \tag{17}$$

where K_p and K_i are the controller proportional and integral coefficients, respectively.

The direct and quadratic currents control structure is illustrated by Fig. 8. The *d*-axis current reference is set to zero in order to minimize Joule losses and, so, minimizing currents for a given torque [47]. Consequently, the generator torque can be directly controlled by the *q*-axis current [48]. The *q*-axis current reference is calculated by the speed loop controller [49].

In open-loop, the division compensation technique allows computing the time-constant T_{OL} by

$$T_{OL} = K_i = \frac{L_S}{R_S} \tag{18}$$

In closed-loop, the time-constant T_{CL} is given by

$$T_{CL} = \frac{R_S K_i}{K_p} \tag{19}$$

Finally, the corrector parameters are the given by

$$\begin{cases} K_i = \frac{L_S}{R_S} \\ K_p = \frac{R_S K_i}{T_{CL}} \end{cases} \tag{20}$$

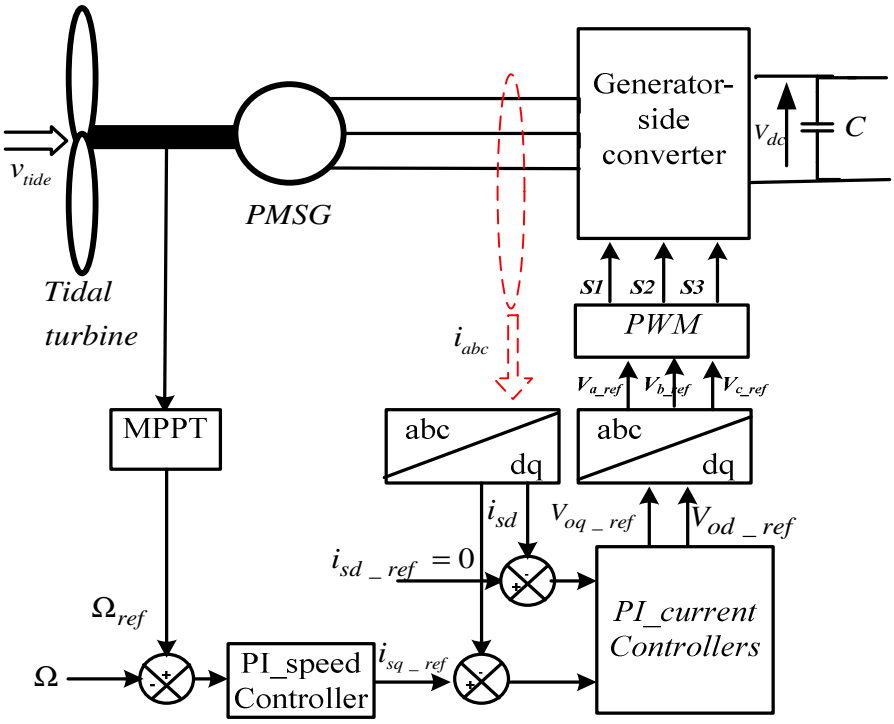

Fig. 6. Generator-side converter control.

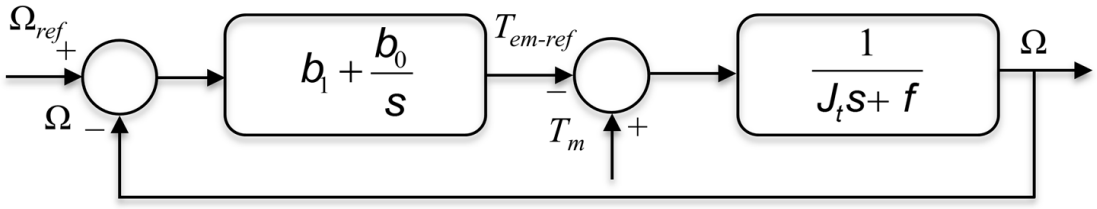

Fig. 7. Control structure of the turbine speed.

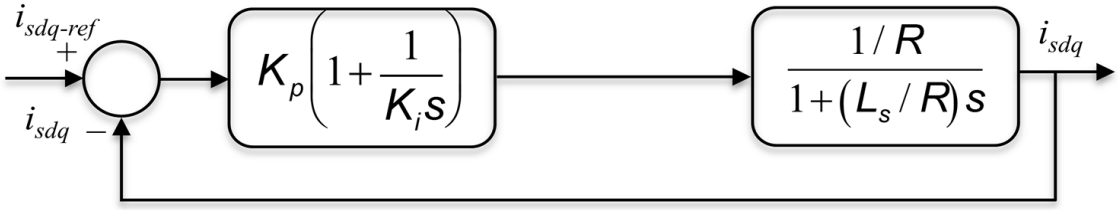

Fig. 8. i_{sdq} currents control structure.

3.2. Grid-side converter control

The grid-side control is illustrated by Fig. 9. It consists in the control of the active power injected to the grid and the reactive power exchanged with the grid.

The active and the reactive powers are given by

$$\begin{cases} P_g = V_{gd} I_{gd} + V_{gq} I_{gq} \\ Q_g = V_{gq} I_{gd} - V_{gd} I_{gq} \end{cases} \tag{21}$$

Or, the *d*-axis is oriented along the grid voltage, so

$$\begin{cases} V_{gd} = V_g \\ V_{gq} = 0 \end{cases} \tag{22}$$

The active and reactive powers are therefore expressed as:

$$\begin{cases} P_g = V_g I_{gd} \\ Q_g = -V_g I_{gq} \end{cases} \tag{23}$$

The active and reactive powers can be directly controlled by the direct and quadratic current components by using two PI controllers. The grid-side converter control is quite similar to that of the generator-side converter.

The reactive power reference is maintained equal to zero ($Q_{q\text{-}ref}$=0) in order to ensure unitary power factor operation. The current controllers give a voltage reference for the converter. A DC voltage controller loop is used to obtain the d-axis current reference for the grid active power control. This ensures that all the power coming from the generator-side converter is immediately transferred to the grid by the grid-side converter.

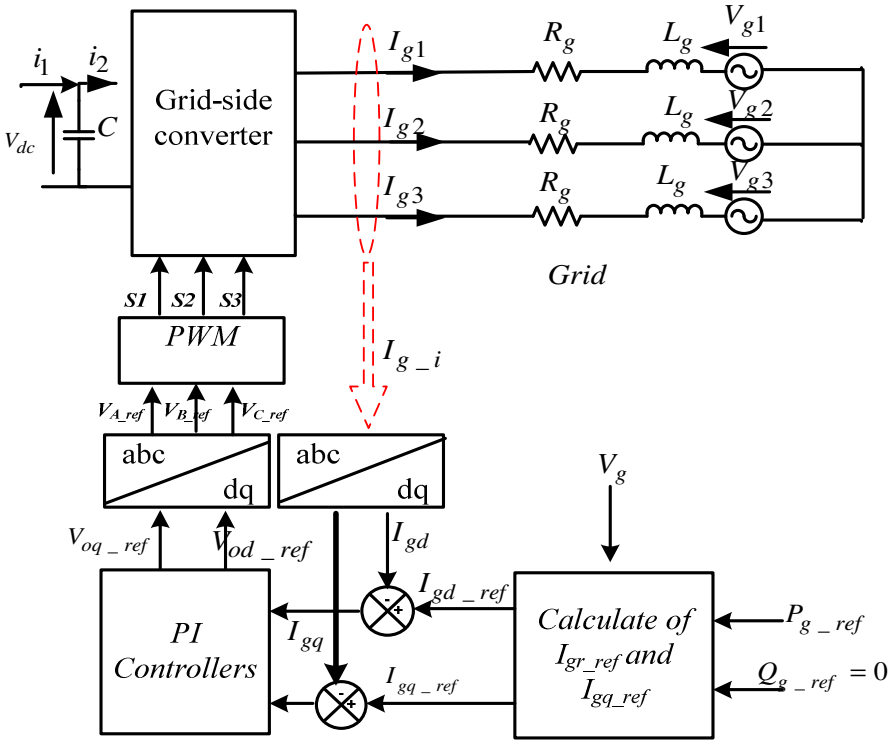

Fig. 9. Grid-side converter control.

3.3. Grid-connected PMSG-based tidal stream turbine post-fault behavior

The tidal stream turbine is located at the Raz de Sein, in Bretagne (France). The simulated grid-connected PMSG-based TST parameters are given in the Appendix. In the simulations, the tidal speed is given for a day (each second represents an hour) (Fig. 10). The grid-connected tidal turbine is simulated using PI controllers.

Figures 11 and 12 depict the PMSG rotor speed and power. A short-circuit grid fault is applied at t= 4s for different amplitudes (20%, 50%, and 70%) of the nominal grid voltage in order to evaluate the impact of the fault severity on the tidal stream turbine behavior. It can be clearly noticed speed ripples as soon as the fault appears. These ripples obviously increase when the fault amplitude increases. At this stage, it seems that a classical PI control is unfortunately not able to efficiently tolerate grid failures. In this case, there is a clear need for more robust control techniques such as the second-order sliding mode.

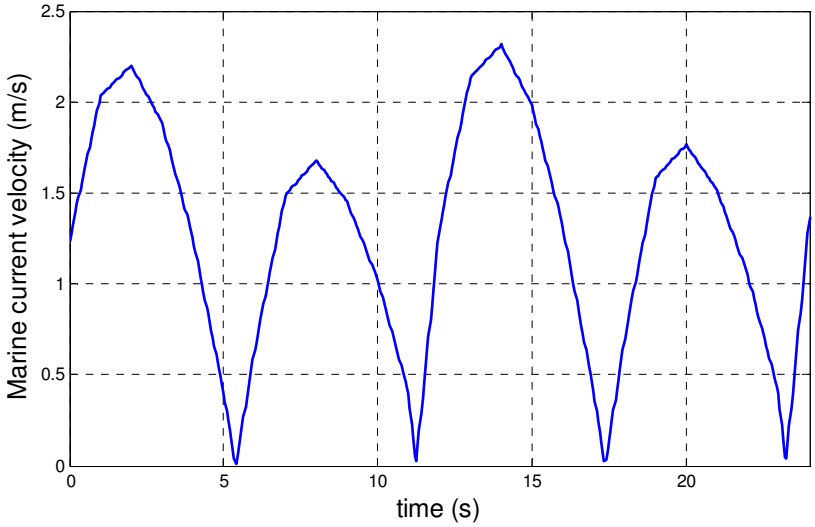

Fig. 10. Marine current velocity.

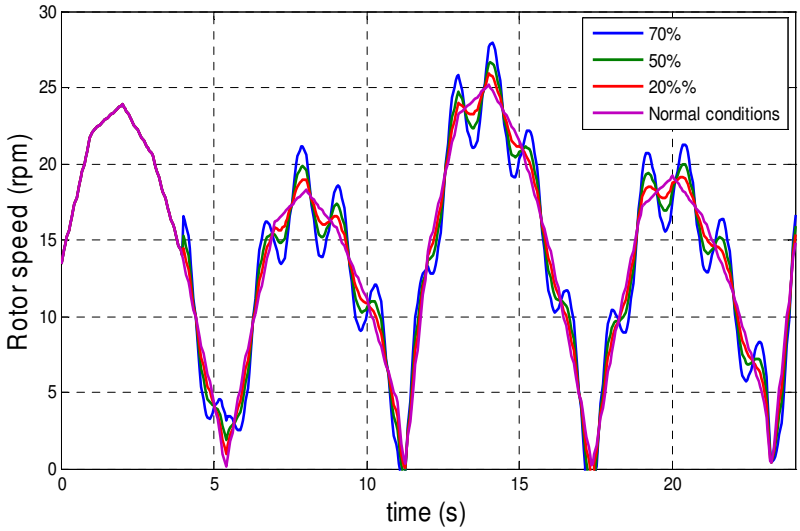

Fig. 11. PMSG rotor speed.

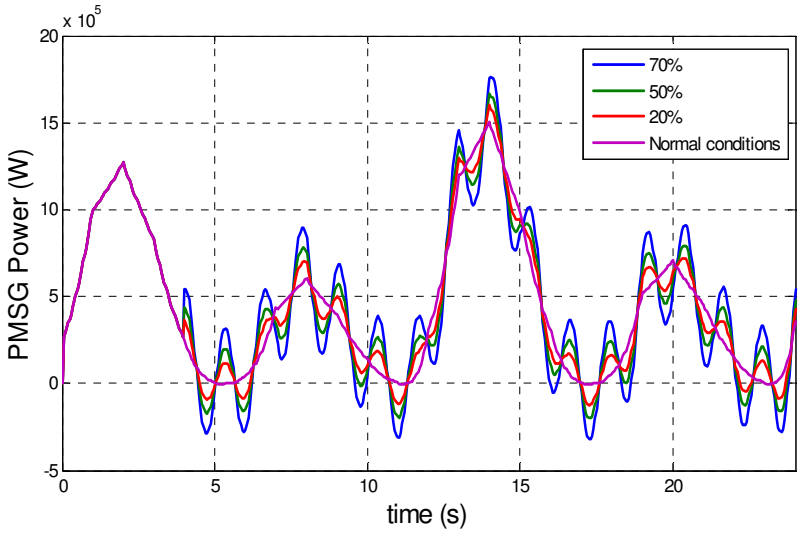

Fig. 12. PMSG power.

4. Grid-connected PMSG-based tidal stream turbine resilient control

In this section, a second-order sliding mode control is adopted. This control presents finite reaching time, attractive features such as chattering-free behavior, and robustness with respect to unmodeled dynamics (turbine and generator), and external disturbances such as grid disturbances.

Sliding mode control is based on moving the system state into sliding surfaces S=0. The aim of second-order sliding mode control is to maintain $S = \dot{S} = 0$, where the system states tends to zero when S and $\dot{S}$ are intersect in the state-space. Second-order sliding mode control is based on the super-twisting algorithm as described in [50].

The active and reactive powers are expressed as

$$\begin{cases} P_g = V_g I_{gd} \\ Q_g = -V_g I_{gq} \end{cases} \tag{24}$$

Or, the reactive power reference is maintained equal to zero ($Q_{q\text{-}ref}$=0), then, the current references are deduced as follows:

$$\begin{cases} I_{gd-ref} = \frac{P_{g-ref}}{V_{gd}} \\ I_{gq-ref} = 0 \end{cases} \tag{25}$$

The proposed control technique algorithm is used to ensure the currents convergence to their references. The sliding surfaces are given by

$$\begin{cases} S_1 = I_{gd} - I_{gd-ref} \\ S_2 = I_{gq} - I_{gq-ref} \end{cases} \tag{26}$$

The derivate of (26) gives

$$\begin{cases} \dot{S_1} = \dot{I_{gd}} - \dot{I_{gd-ref}} \\ \ddot{S_1} = \varphi_1(t,x) + \gamma_1(t,x) V_{gd} \end{cases} \tag{27}$$

and

$$\begin{cases} \dot{S_2} = \dot{I_{gq}} - \dot{I_{gq-ref}} \\ \ddot{S_2} = \varphi_2(t,x) + \gamma_2(t,x) V_{gq} \end{cases} \tag{28}$$

where $\varphi_1(t,x)$, $\varphi_2(t,x)$, $\gamma_1(t,x)$ and $\gamma_2(t,x)$ are uncertain bounded functions that satisfy

$$\begin{cases} \varphi_1 > 0;\ |\varphi_1| > \Phi_1; 0 < \Gamma_{m1} < \gamma_1 < \Gamma_{M1} \\ \varphi_2 > 0;\ |\varphi_2| > \Phi_2; 0 < \Gamma_{m2} < \gamma_2 < \Gamma_{M2} \end{cases} \tag{29}$$

where$\Gamma_{m1}$and $\Gamma_{M1}$are the lower and the upper bounds of γ_1, respectively, while Γ_{m2} and Γ_{M2} are the lower and the upper bounds of γ_2, respectively.

The proposed second-order sliding mode controller has two parts [45]

$$\begin{cases} V_{gd} = u_1 + u_2 \\ V_{gq} = w_1 + w_2 \end{cases} \tag{30}$$

where

$$\begin{cases} \dot{u_1} = -\alpha_1 sign\,(S_1) \\ u_2 = -\beta_1 |S_1|^{\xi} sign\,(S_1) \end{cases} \tag{31}$$

and

$$\begin{cases} \boldsymbol{\dot{w}_1 = -\alpha_2 sign\,(S_2)} \\ \boldsymbol{w_2 = -\beta_2 |S_2|^{\xi} sign\,(S_2)} \end{cases} \tag{32}$$

where α_1, α_2, β_1, and β_2 are gains.

To ensure the convergence of the sliding manifolds to zero in finite-time, the gains can be chosen as follows.

$$\begin{cases} \alpha_i > \frac{\Phi_i}{\Gamma_{mi}} \\ \beta_i^2 \geq 4 \frac{\Phi_i}{\Gamma_{mi}^2} \frac{\Gamma_{Mi}}{\Gamma_{mi}} \frac{(\alpha_i + \Phi_i)}{(\alpha_i - \Phi_i)}; \;\; i = 1, 2 \\ 0 < \xi \leq 0.5 \end{cases} \tag{33}$$

5. Simulation results

In this section, the grid-connected PMSG-based tidal stream turbine is simulated using both PI controllers and second-order sliding mode control strategy. The short-circuit grid fault amplitude is 70% of the nominal grid voltage.

Figures 13, 14, 15, and 16 depict the PMSG rotor speed, the PMSG power, the grid power, and the reactive power, respectively. At fault occurrence (at t=4s), it can clearly be seen that, by using PI controllers, these curves show some ripples, while, with second-order sliding mode control; the tidal turbine system power and dynamic performances are almost degradation-free.

At fault occurrence (t=0.1s), grid currents are increased to high values (Fig. 17), which generally leads to the system being turned off. At t= 0.3s, the fault-resilient control is applied, so, grid currents go back to their initials states. Consequently, these results obviously confirm that the second-order sliding mode out performs PI controllers in terms of grid failure resilience effectiveness.

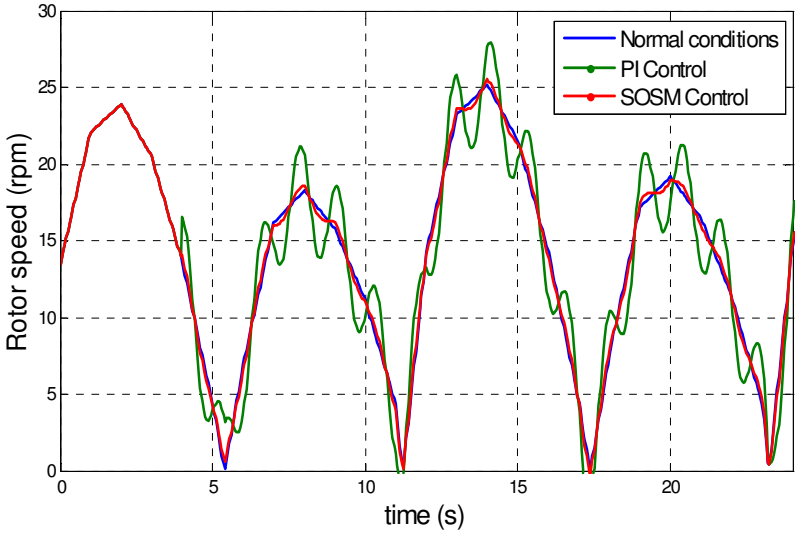

Fig. 13. PMSG Rotor speed.

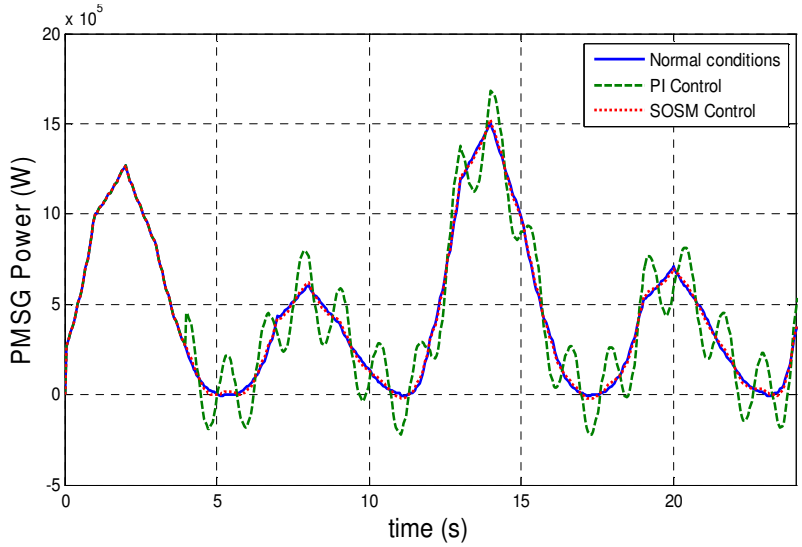

Fig. 14. PMSG power.

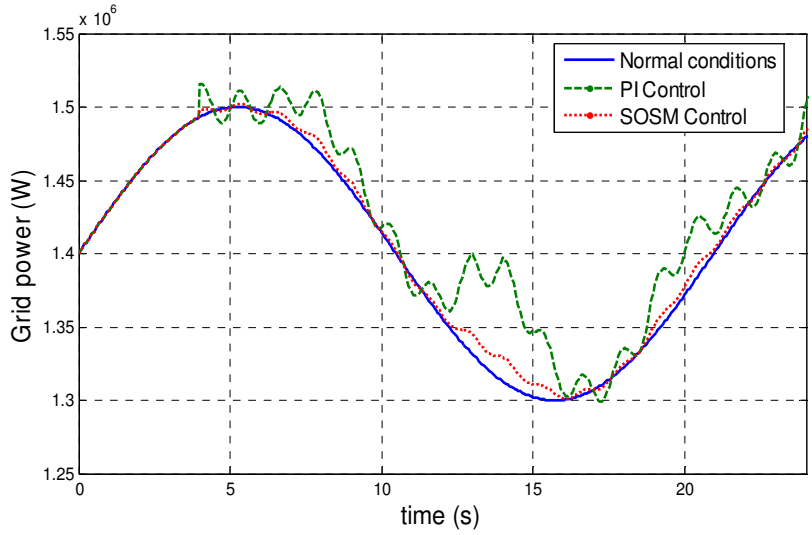

Fig. 15. Grid power.

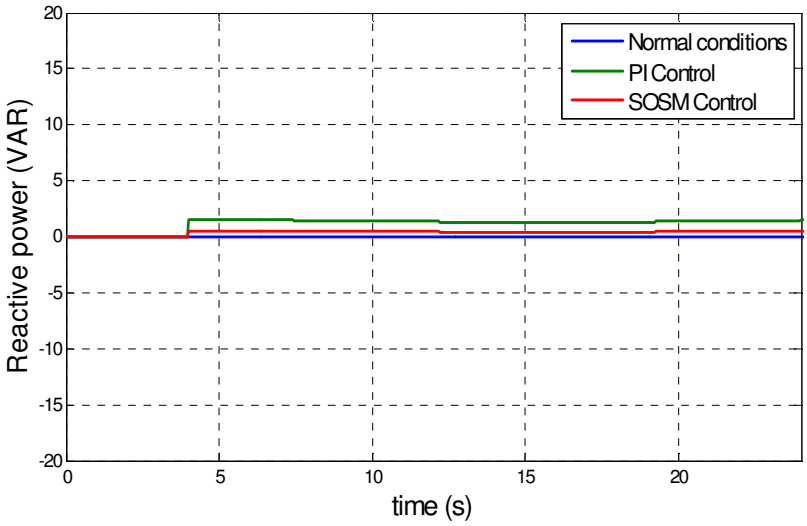

Fig. 16. Grid reactive power.

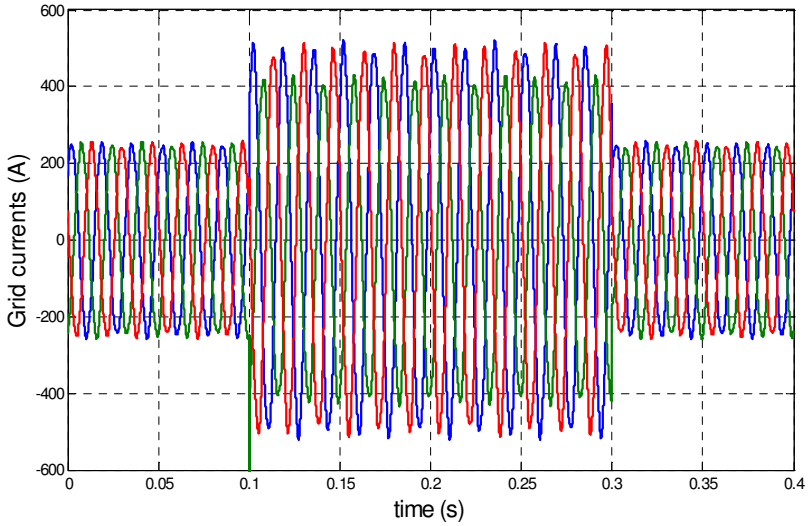

Fig. 17. Grid currents.

6. Conclusion

This paper has presented and analyzed grid fault effect on a grid-connected PMSG-based tidal stream turbine. Primary simulation results have shown that the tidal stream turbine system both generated power and dynamic performances are negatively impacted by the grid fault when using conventional PI controllers. To overcome this issue, a robust and grid-resilient control technique, namely a second-order sliding mode, has been adopted. The achieved performance results have shown that a second-order sliding mode control performance clearly outperforms PI controllers even if they are optimally designed. These results obviously confirm that high-order sliding modes control is the solutions of choice for a tidal stream turbine.

Further investigations should however be carried out toward more recent robust control techniques, such as the active disturbance rejection control that has been recently tested for a tidal stream turbine under healthy conditions and for a PMSG-based electric vehicle under fault conditions.

Appendix: Grid-connected tidal turbine parameters

	Parameter	Value
Tidal turbine	Radius	8m
	Number of blades	3
	Fluid density	1027.68kg/m^3
PMSG	Rated power	1.5MW
	Rated speed	25rpm
	Stator resistance	0.0081Ω
	d-axis inductance	1.2mH
	q-axis inductance	1.2mH
	Permanent magnets flux	2.458Wb
	System total inertia	1.3131x10^{6}kg.m^2
	Viscosity coefficient	8.5 10^{-3}Nm/s
Converters	Turn-on time	0.13µs
	Turn-off time	0.445µs
	Dead-time	4µs
	Duty-cycle frequency	5kHz
DC Bus	Capacitor	13mF
Grid	Resistance	0.1mΩ
	Inductance	1.5mH
	Frequency	50Hz

References

[1] M. E. H. Benbouzid, H. Titah-Benbouzid, and Z. Zhou, Ocean Energy Technologies. In: Abraham, M.A. (Ed.), *Encyclopedia of Sustainable Technologies*. Elsevier, pp. 73-85, ISBN: 978-0-128-04677-7, 2017.

[2] M. E. H. Benbouzid, Y. Amirat, and E. Elbouchikhi, (Eds), *Marine Tidal and Wave Energy Converters Technologies: Conversions, Grid Interface, Fault Detection, and Fault-Tolerant Control*, Energies Special Issue Reprint, ISBN 978-3-03928-279-1, MDPI, Basel 2020.

[3] ENTSO-E Incident Reports, https://www.entsoe.eu/publications/system-operations-reports/ (last accessed April 2020).

[4] M. E. H. Benbouzid, M. S. Muyeen, and F. Khoucha, "An up-to-date review of low-voltage ride-through techniques for doubly-fed induction generator-based wind turbines," *International Journal on Energy Conversion*, vol. 3, n°1, pp. 1-9, January 2015.

[5] M. E. H. Benbouzid, B. Beltran, Y. Amirat, G. Yao, J. Han, and H. Mangel, "Second-order sliding mode control for DFIG-based wind turbines fault ride-through capability enhancement," *ISA Transactions*, vol. 53, n°3, pp. 827-833, May 2014.

[6] L. Zhang, X. Cai, and J. Guo, "Dynamic response of DFIG fault currents under constant AC excitation condition," *in Proceedings of the 2009 IEEE APPEEC, 2009*, Whuhan (China), pp. 1-6, March 2009.

[7] A. Mullane, G. Lightbody, R. Yacamii, "Wind turbine fault ride through enhancement,"*IEEE Trans. Power Systems*, vol. 20, n°4, pp. 1929-1937, 2005.

[7] F. Endrejat and P. Pillay, "Ride-through of Medium Voltage Synchronous Machine compressor drives," *in Proceedings of the 2009 IEEE IEMDC*, Miami (USA), pp. 909–915, May 2009.

[8] A. van Zyl, R. Spee, A. Faveluke, and S. Bhowmik, "Voltage sag ride-through for adjustable speed drives with active rectifiers," *in Proceedings of the 1997 IEEE IAS Annual Meeting*, New Orleans (USA), vol. 1, pp. 486–492, October 1997.

[9] S. S. Deswal, R. Dahiya, and D. K. Jain, "Ride-through alternatives of Adjustable Speed Drives (ASD's) during fault conditions," *in Proceedings of the 2010 Joint IEEE PEDES – Power India*, New Delhi (India) pp. 1–7, December 2010.

[10] H. J. N. Ndjana, P. Sicard, S. Lahaie, and E. Ngandui, "Auxiliary voltage sag ride through system for adjustable-speed drives," *in Proceedings of the 2005 IEEE IEMDC*, San Antonio (USA), pp. 450–457, May 2005.

[11] E. P. Wiechmann, R. P. Burgos, and J. Rodriguez, "Continuously motor-synchronized ride-through capability for matrix-converter adjustable-speed drives," *IEEE Trans. Industrial Electronics*, vol. 49, n°2, pp. 390–400, April 2002.
[12] K. Stockman, F. D'hulster, K. Verhaege, M. Didden, and R. Belmans, "Ride-through of adjustable speed drives during voltage dips," *Electric Power Systems Research.*, vol. 66, n°1, pp. 49–58, July 2003.
[13] Z. Zhou, F. Scuiller, J. F. Charpentier, M. E. H. Benbouzid, and T. Tang, "Power smoothing control in a grid-connected marine current turbine system for compensating swell effect," *IEEE Trans. Sustainable Energy*, vol. 4, n°3, pp. 816-826, July 2013.
[14] S.I. Gkavanoudis and C. S. Demoulias, "A combined fault ride through and power smoothing control method for full-converter wind turbines employing supercapacitor energy storage system," *Electric Power Systems Research*, vol. 106, pp. 62–72, January 2014.
[15] H. T. Pham, J. M. Bourgeot, and M. E. H. Benbouzid, "Power smoothing control and low-voltage ride-through enhancement of a 5-phase PMSG-based marine tidal turbine using a supercapacitor energy storage system," *in Proceedings of the 2017 IEEE IECON*, Beijing (China), pp. 8323-8328, October-November 2017.
[16] J. Morren, S. W. H. de Hann, "Ride through of wind turbines with doubly-fed inductiongenerator during a voltage dip,"*IEEE Trans. Energy Conversion*, vol. 20, n°2, pp. 435-441, June 2005.
[17] A. Hansen and G. Michalke, "Fault ride-through capability of DFIG wind turbines,"*Renewable Energy,* vol. 32, n°9, pp. 1594–1610, July 2007.
[18] G. Pannell, D. J. Atkinson, and B. Zahawi, "Minimum-threshold crowbar for a fault-ride-through grid-code-compliant DFIG wind turbine," *IEEE Trans. Energy Conversion*, vol. 25, n°3, pp. 750–759, Sep. 2010.
[19] J. Yang, J. O'Reilly, and J. E. Fletcher, "Protection scheme switch-timing for doubly fed induction generator during fault conditions," in Proceedings of the 2009 IEEE *PowerTech*, Bucharest (Romania), pp. 1–6, July 2009.
[20] L. Peng, B. Francois, and Y. Li, "Improved crowbar control strategy of DFIG based wind turbines for grid fault ride-through," *in Proceedings of the 2009 IEEE APEC*, pp. 1932–1938, February 2009.
[21] M. Wang, W. Xu, H. Jia, and X. Yu, "A new method for DFIG fault ride through using resistance and capacity crowbar circuit," *in Proceedings of the 2013 IEEE ICIT*,Cape Town (South Africa), pp. 2004–2009, February 2013.
[22] D. Ramirez, S. Martinez, F. Blazquez, and C. Carrero, "Use of STATCOM in wind farms with fixed-speed generators for grid code compliance," *Renewable Energy*, vol. 37,n°1, pp. 202–212, January 2012.
[23] M. Muthusamy and C. S. Kumar, "New STATCOM control scheme for power quality improvement in wind farm," *in Proceedings of the 2014 IEEE ICGCCEE*, Coimbatore (India), pp. 1–5, March 2014.
[24] P.S. Flannery and G. Venkataramanan, "A fault tolerant doubly fed induction generator wind turbine using a parallel grid side rectifier and series grid side converter," *IEEE Trans. Power Electronics*, vol. 23, n°3, pp. 1126–1134, May 2008.
[25] D. Xiang, Li. Ran, P.J. Tavner, S. Yang, "Control of a doubly fed induction generator in a wind turbine during grid fault ride-through," *IEEE Trans. Energy Conversion*, vol. 21, n°3,pp. 652–662, September 2006.
[26] M. Rahti and N. Mohan, "A novel robust low voltage and fault ride through for wind turbine application operating in weak grids," *in Proceedings of the 2005 IEEE IECON*, Raleigh (USA), pp. 1-6, November 2005.
[27] J. Mohammadi, S. Afsharnia, and S. Vaez-Zadeh, "Efficient fault-ride-through control strategy of DFIG-based wind turbines during the grid faults," *Energy Conversion and Management*,vol. 78, pp. 88–95, February 2014.
[28] M. Mohseni, M. A. S. Masoum, and S. M. Islam, "Low and high voltage ride-through of DFIG wind turbines using hybrid current controlled converters," *Electric Power Systems Research*, vol. 81, n°7, pp. 1456–1465, July 2011.
[29] S. Xiao, G. Yang, H. Zhou, and H. Geng, "An LVRT control strategy based on flux linkage tracking for DFIG-based WECS," *IEEE Trans. Industrial Electronics*, vol. 60, n°7, pp. 2820–2832, July 2013.
[30] R. Zhu, Z. Chen, X. Wu, and F. Deng, "Virtual damping flux-based LVRT control for DFIG-based wind turbine," *IEEE Trans. Energy Conversion*, vol. 30, n°2, pp. 714–725, June 2015.
[31] T. D. Vrionis, X. I. Koutiva, and N. A. Vovos, "A genetic algorithm-based low voltage ride-through control strategy for grid connected doubly fed induction wind generators," *IEEE Trans. Power Systems*, vol. 29, n°, pp. 1325–1334, May 2014.
[32] S. Toumi, Y. Amirat, M. Trabelsi, E. Elbouchikhi, M.F. Mimouni, and M.E.H Benbouzid, "Backstepping Control of a PMSG-based marine current turbine system under Faulty conditions," *in Proceedings of the 2018 IEEE IREC*, Hammamet (Tunisia), pp. 1-6, Mars 2018.
[33] French Navy Hydrographic and Oceanographic Service [Online], 2018. Available: www.shom.fr/
[34] S. Toumi, Y. Amirat, E. Elbouchikhi, M. Trabelsi, M.E.H. Benbouzid, and, M.F. Mimouni, "A comparison of fault-tolerant control strategies for a PMSG-based marine current turbine system under converter faulty conditions," *Journal of Electrical Systems*, vol. 13, n°3, pp. 472-488, June 2017.
[35] S. Toumi, S. Ben Elghali, M. Trabelsi, E. Elbouchikhi, M.E.H. Benbouzid, and M.F. Mimouni, "Robustness analysis and evaluation of a PMSG-based marine current turbine system under faulty conditions," *in Proceedings of the 2014 IEEE STA*, Hammamet (Tunisia), pp. 631-636, December 2014.

[36] S. Toumi, Y. Amirat, E. Elbouchikhi, M. Trabelsi, M. F. Mimouni, and M. E. H Benbouzid, "Second-order sliding mode for marine current turbine fault-tolerant control," *in Proceedings of the 2016 IEEE CEIT*, Hammamet (Tunisia), pp. 1-6, December 2016.
[37] S. Toumi, E. Elbouchikhi, Y. Amirat, M. E. H. Benbouzid, and G. Feld, "Magnet failure-resilient control of a direct-drive tidal turbine," *Ocean Engineering*, vol. 187, 106297, pp. 1–10, September 2019.
[38] Z. Zhou, F. Scuiller, J. F. Charpentier, M. E. H. Benbouzid, and T. Tang, "Power control of a nonpitchable PMSG-based marine current turbine at overrated current speed with flux-weakening strategy," *IEEE Journal of Oceanic Engineering*, vol. 40, n°3, pp. 536-545, October 2015.
[39] H. T. Pham, J.M. Bourgeot and M. E. H. Benbouzid, "Comparative investigations of sensor fault-tolerant control strategies performance for marine current turbine applications," *IEEE Journal of Oceanic Engineering*, vol. 43, n°4, pp. 1024–1036, October 2018.
[40] S. Toumi, S. Ben Elghali, M. Trabelsi, E. Elbouchikhi, Y. Amirat, M.E.H. Benbouzid, and M.F. Mimouni, "Modeling and simulation of a PMSG-based marine current turbine system underfaulty rectifier conditions," *Electric Power Components and Systems*, vol. 45, n°7, pp. 715-725, April 2017.
[41] S. Benelghali, M.E.H. Benbouzid, and J. F. Charpentier, "Generator systems for marine current turbine applications: A comparative study," *IEEE Journal of Oceanic Engineering*, vol. 37, n°3, pp. 554-563, July 2012.
[42] S. Toumi, Y. Amirat, E. Elbouchikhi, M. Trabelsi, M. E. H Benbouzid, and M. F. Mimouni, "A simplified mathematical approach for magnet defects modeling in a PMSG used for marine current turbine," *in Proceedings of the 2016 IEEE STA*, Sousse (Tunisia), pp. 1-6, December 2016.
[43] S. Toumi, E. Elbouchikhi, Y. Amirat, M. Trabelsi, M.E.H. Benbouzid, and M.F. Mimouni, "Marine current turbine system post-fault behavior under an open circuit fault," *Advances in Electrical and Electronic Engineering*, vol. 16, n°3, pp. 279-287, September 2018.
[44] M. Esselin, B. Robyns, F. Berthereau, and J.P Hautier, "Resonant controller based power control of an inverter transformer association in a wind generator", *Electromotion*, vol. 7, n°4, pp. 185-190, 2000.
[45] M. Chinchilla, S. Arnaltes, and J. C Burgos, "Control of permanent-magnet generators applied to variable-speed wind-energy systems connected to the grid," *IEEE Trans. Energy Conversion*, vol. 21, n°1, pp. 130-135, March 2006.
[46] Z. Wang, J. Chen, M. Cheng, and Y. Zheng, "Fault tolerant control of paralleled voltage-source inverters fed PMSM drives," *IEEE Trans. Industrial Electronics*, vol. 62, n°8, pp. 4749-4760, August 2015.
[47] A. Ansel and B. Robyns, "Modelling and simulation of an autonomous variable speed micro hydropower station," *Mathematics and Computers in Simulation,* vol. 71, n°4-6, pp. 320-332, 2006.
[48] Z. Wang, B. Wu, D. Xu, and N. R. Zargari, "A current -source-converter-based high-power high-speed PMSM drive with 420-Hz switching frequency," *IEEE Trans. Industrial Electronics*, vol. 59, n°7, pp. 2970-2981, July 2012.
[49] S. Chi, Z. Zhang, and L. Xu, "Sliding-mode sensorless control of direct-drive PM synchronous motors for washing machine applications," *IEEE Trans. Industry Applications*, vol. 45, n°2, pp. 582-590, March-April 2009.
[50] Z. Zhou, S. Ben Elghali, M. E. H. Benbouzid, Y. Amirat, E. Elbouchikhi, and G. Feld, "Tidal stream turbine control: An active disturbance rejection control approach," *Ocean Engineering*, vol. 202, Article 107190, pp. 1–9, April 2020.